The MROI Fringe Tracker: First Fringe Experiment

C. Jurgenson*[a], F. Santoro[a], T. McCracken[a], K. McCord[a], A. Shtromberg[a], D. Klinglesmith[a], A. Olivares[a], D. Buscher[b], M. Creech-Eakman[a], C. Haniff[b], J. Young[b]
[a]Magdalena Ridge Observatory, 101 East Road, Socorro, NM, USA 87801;
[b]Cavendish Laboratory, University of Cambridge, J.J. Thomson Avenue, Cambridge, CB3 OHE, UK

ABSTRACT

The MROI fringe tracking beam combiner will be the first fringe instrument for the interferometer. It was designed to utilize the array geometry and maximize sensitivity to drive the interferometer for faint source imaging. Two primary concerns have driven the design philosophy: 1) maintaining high throughput and visibilities in broadband polarized light, and 2) mechanical stability. The first concern was addressed through tight fabrication tolerances of the combiner substrates, and custom coatings. In order to optimize mechanical stability, a unique modular design approach was taken that minimizes the number of internal adjustments. This paper reports initial laboratory fringe and stability measurements.

Keywords: MRO, interferometry, fringe tracking, baseline bootstrapping image, group delay

1. INTRODUCTION

This paper seeks to report advancements in the optomechanical development of the MROI fringe tracker from a previous description[1]. The sole function of this system is to keep the array in phase over its intended 45 independent baselines, enabling the focus of the science combiners to be on maximizing the science product. It does this by stabilizing the fringes on shorter "nearest neighbor" baselines, and thus allowing for increased integration times on the longer baselines and the build-up of signal to noise. In addition, the optics and coatings have been optimized for either H or K_s-Band operation, allowing for the instrument to operate in a separate bandpass from the science combiners. Every aspect of its design, from beam combiner architecture to thin film coatings, has implemented ways to not only maximize throughput, but wavefront quality, and therefore increased fringe visibility[2].

1.1 System Components

There are four fundamental optomechanical subsystems that make up the fringe tracker:

1. Switchyard: configures the input phase plane to match that expected by the combiner; used to remove tilt and shear errors between combination partners in the combination plane.
2. Beam Combiner: takes inputs from the switchyard and makes the intended nearest neighbor combinations to bootstrap the array.
3. Periscope Optics: folds the beam combiner output pattern to multiplex up to five combinations onto a single detector; ensures the outputs are not vignetted by the pinholes inside the spectrograph.
4. Spectrograph: spatially filters, and spectrally disperses the combiner outputs into five spectral channels onto the detector.

Figure 1 is the scaled 3-D optomechanical design of the fringe tracker and its subsystems. In the figure, ten beams traverse through the system upon exiting the vacuum delay lines[3]. At lower right in the figure, the two reflection switchyard inputs the beams into the combiner with the intended phase plane and beam pitch. Upon exiting the beam combiner, the periscope optics fold up to five combiner outputs into an arc for delivery into the spectrographs. Two sets of periscope optics and spectrographs are needed to accommodate the two combiner outputs. Since one spectrograph can only accept five combiner outputs, a total of four will be needed when the array is operating with its full complement of 10 unit telescopes. The back end of the spectrograph is a Teledyne PICNIC array.

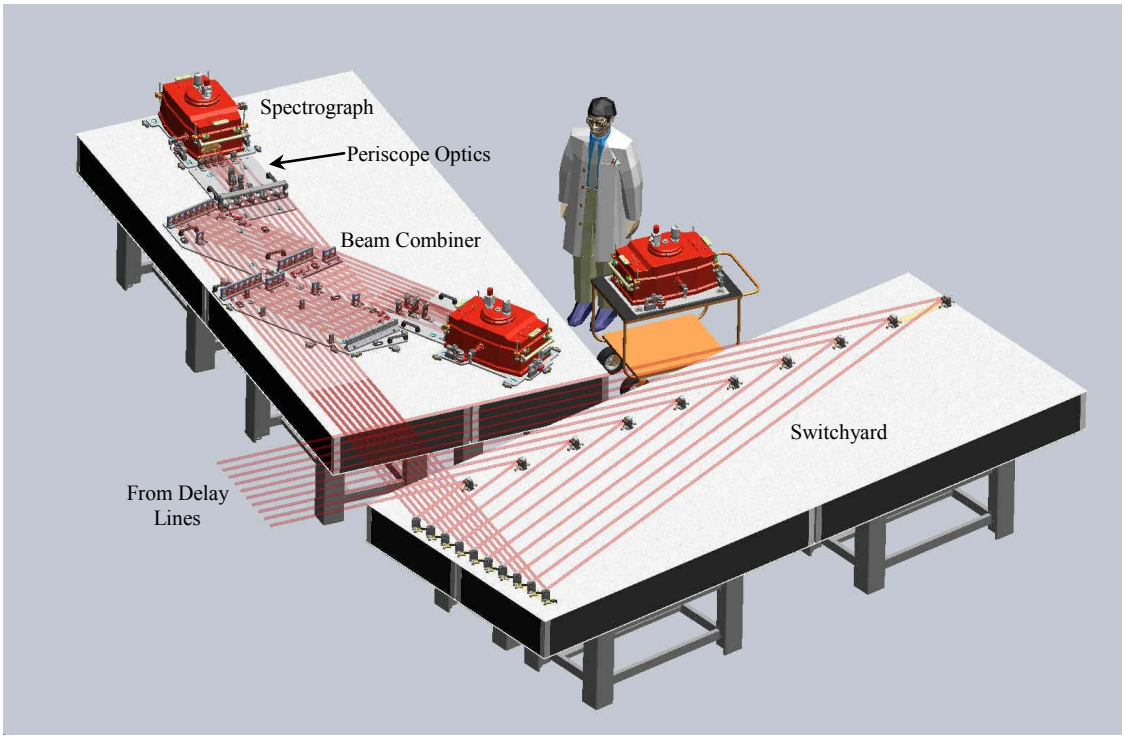

Figure 1. Overview of the optomechanical design of the MROI fringe tracker and its subsystems. Beams enter the switchyard from the delay lines, and undergo a figure-4 reflection in the switchyard before entering the beam combiner. Following the beam combiner, the periscope folds the outputs into an arc pattern for injection into the spectrographs.

1.2 Combiner Architecture

The baseline bootstrapping technique as applied to the MROI is illustrated in Figure 2. At left in the figure, telescope stations (represented as circles) are numbered 1 (inner), 2 (middle), and 3 (outer) within a given arm N (North), S (South), or W (West). The short arrows in between the circles represent the nearest neighbor combinations that are made to bootstrap the array from the outer to the inner telescopes within a given arm, and then from the inner telescopes through the central (W0) to phase up the three arms. The right hand side of Figure 2 illustrates the resulting combiner architecture.

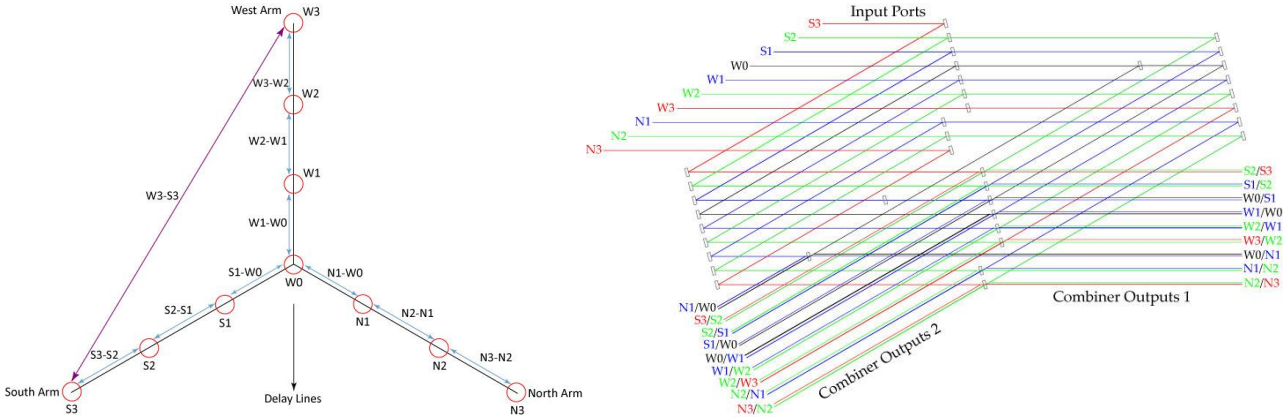

Figure 2. Bootstrapping the MROI. *Left:* Illustration of the array geometry. *Right:* Resulting combiner architecture.

1.3 Spectrograph

The primary function of the spectrograph is to:

1. Spatially filter the combiner outputs
2. Spectrally disperse them
3. Detect the dispersed fringe patterns

It has been optimized to operate in either H or K_s-Band (does not share light with science combiner), and can multiplex up to five combiner outputs onto a single detector. The detector is a Teledyne PICNIC array, with 256x256 pixels and 40μm pixel pitch. Figure 3 shows the critical optomechanical design.

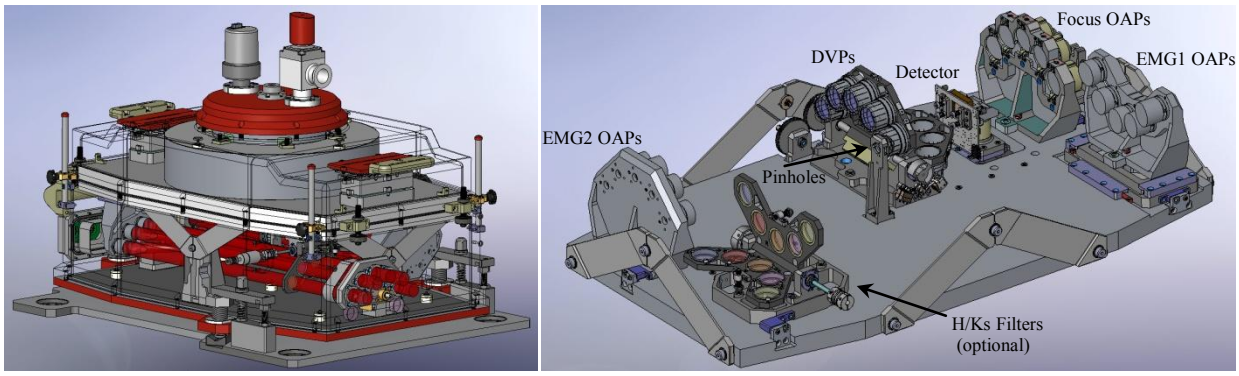

Figure 3. Two views of the critical spectrograph design. *Right:* Dewar design highlighting the LN2 tank (enclosure transparent) interfacing to the cold-working surface plate. Combiner outputs are entering through the dewar windows in an arc pattern at lower right. *Left:* Optics and their mounts on the cold-working surface plate. The optics are all reflective (except for dispersing elements), OAPs.

With the exception of the direct view prisms (DVPs), the optics are all reflective, off-axis parabolas (OAPs). OAPs in an Eccentric Mersenne Gregorian (EMG) configuration focus the beams through pinholes (EMG1) and then recollimate them (EMG2) before dispersion. Flipper mechanisms are used to select either H or K_s optimized DVPs. Currently there are no plans to use spectral filters, but the capability will be available if necessary. In Section 1.1 it was noted that the periscope optics fold the combiner outputs into an arc so that they can be multiplexed onto a single detector. This arc pattern is carried all the way through to the detector.

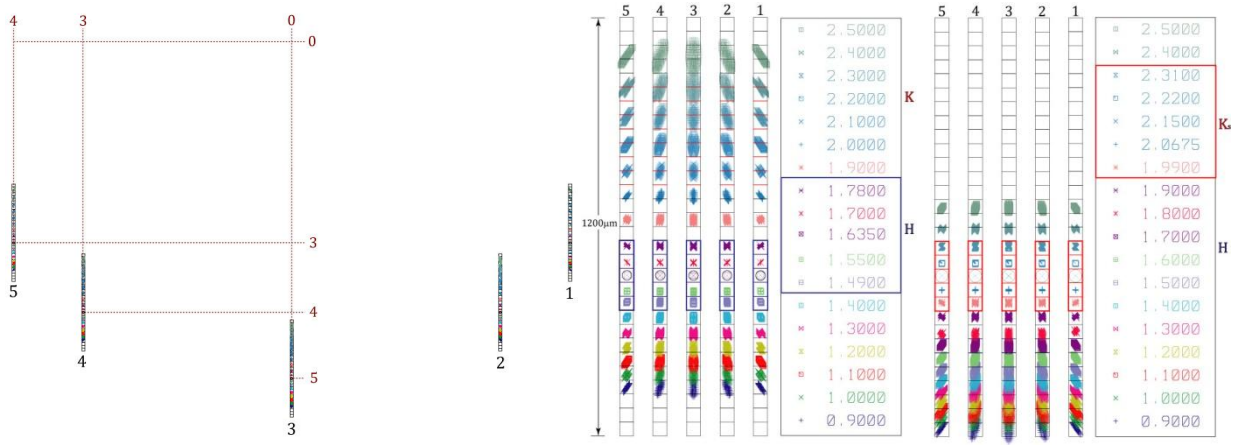

Figure 4. *Left:* Spatial relationship on the detector for a given five combiner outputs. *Right:* Spot diagrams for the different DVP optimized bands (H at left, K_s at right). The five spectral channels to be read out are bounded by the rectangles. Note that the spots within those five spectral channels are diffraction limited to within a pixel.

Figure 4, left, is a scaled spot diagram of the H-Band dispersed outputs as they would appear on the detector (K_s band will have the same spatial arrangement). The different outputs are situated on the array to form a 3-4-5 triangle. Since

there isn't any spectral filtering, light across all wavelengths from J through K will be sensed be the detector. At right in Figure 4 shows the five dispersed outputs for the H-Band optimized DVPs (left), and the K_s-Band optimized DVPs (right). Each box is representative of the PICNIC pixel size. In both cases the same five spectral channels are read out, and these are highlighted in the figure by the boxes bounding the pixels. The optical design calls for diffraction limited performance (Airy disk within a pixel) across both bands for the five spectral channels.

1.4 System Architecture

Figure 5 is an overview of how the system functions as an entity. In this simplified case light from three telescopes (N1/W0/S1) enters the combiner, and two pairs of outputs, π radians out of phase (e.g. N1-W0/W0-N1), enter the spectrograph. The spectrograph disperses the four fringe patterns into five spectral channels onto a detector. This constitutes the 0 and π measurements (A and C) in the A,B,C, and D modulation scheme. Once the four columns of five pixels are read out by the system "brain," it then instructs the beam combiner to modulate (step)[4] the input beams in phase by π/2 radians to get the two remaining B and D measurements. The process of reading out the detector is then repeated, and the "brain" has enough information to determine the group delay which is used to calculate the delay offsets to be applied to the delay lines. In this case, bootstrapping is done through W0, so the offsets are only applied to N1 and S1.

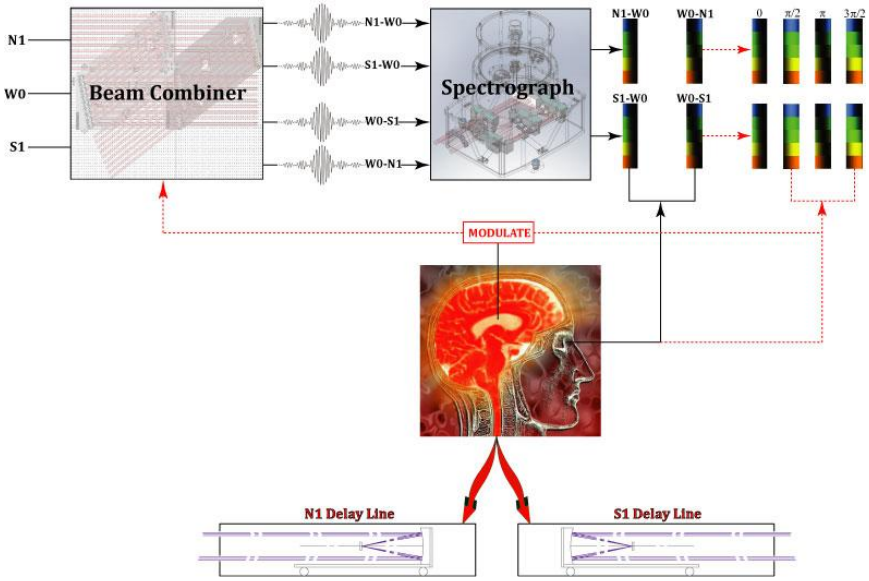

Figure 5. Schematic illustrating the function of the fringe tracking system. In this case, light from three telescopes enters the combiner and four complimentary outputs are dispersed into 5 spectral channels by the spectrograph. After modulation, all four A, B, C, and D measurements have been made, and delay offsets are then applied to the N1 and S1 delay lines. In this case, bootstrapping is done through W0.

2. FIRST FRINGE EXPERIMENT

2.1 Purpose

The first fringe experiment was originally conceived to perform initial tests on key design aspects of not only the beam combiner, but the interferometer calibration systems[5]. These tests were defined to be:

1. Beam Combiner
    - Internal alignment methodology
    - Mechanical stability
    - Fringe contrast

2. Calibration Systems[5]

- Tilt/shear alignment algorithms
- OPD calibration algorithms

An IR laser diode has been used initially to verify the internal alignment method, test mechanical stability, verify the tilt/shear algorithms, and generate fringes. The next phase will use a fiber based system to inject broadband light into the combiner to generate white light fringes and test OPD calibration algorithms. Figure 6 highlights the key components of the first fringe experimental design. A fiber-based white light injection system feeds light into the mock switchyard which inputs two beams with the correct phase plane and beam pitch into the combiner. The mock periscope optics are then position at the appropriate combiner output, and direct it toward the tilt/shear cameras. Positioning templates have been fabricated to allow for quick relocation of the mock switchyard and periscope optics so that different inputs and outputs can be interrogated.

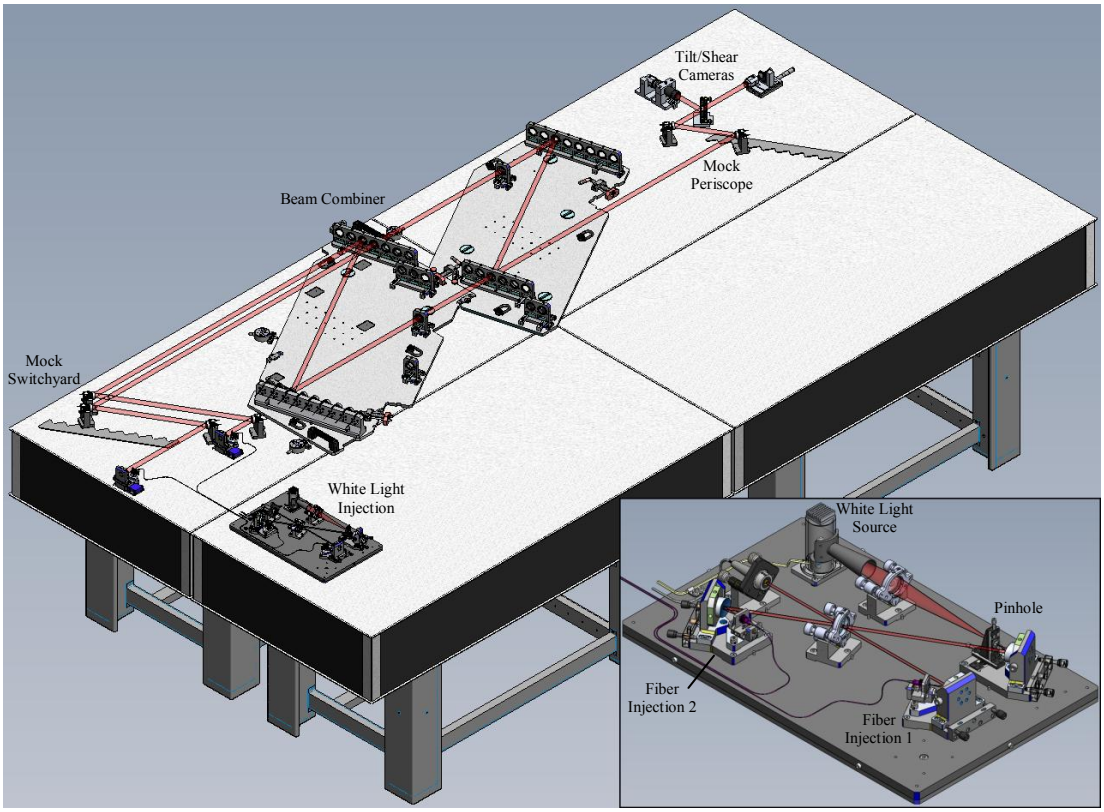

Figure 6. First fringe experiment design. A fiber-based system injects white light into the combiner, and tilt/shear cameras are positioned at the output. The experimental set-up allows for the interrogation of any combiner input/output, as well as path modulation of one of the input beams for determining the position of the peak fringe intensity.

Inset at lower right in the figure is a close-up view of the white light injection system. The filament of a white light source is reimaged onto a pinhole, and then collimated before being split by and beamsplitter and injected into two fibers (Fiber Injection 1 and 2). These fibers are then fed to separate collimating OAPs positioned on automated slides. Collimated light from the slide OAPs become the inputs into the mock switchyard. To locate the zero path difference, one of the slides is modulated with respect to the other, and the slide encoder position corresponding to the peak fringe intensity from the shear camera is recorded.

2.2 Experimental Set-up

Figure 7 is the current experimental set-up in the laboratory. A 1550nm laser diode is being used as the initial light source. Fabrication of the white light fiber injection system described above will be installed as soon as fabrication is

complete (later this Summer). Light from the laser diode is first split by a beamsplitter and injected into two separate inputs of the mock switchyard. In the figure, the mock switchyard is positioned to send light into the N1/N2 (recall Figure 2) combiner inputs. An H-Band camera is currently parked at the output. The stepped plate attached to the table in the mock switchyard is the positioning template that allows for all combiner inputs/outputs to be tested. Also located in the figure is the modulator bank. This is where the inputs are modulated[4] to get the A, B, C, D phase measurements described in Section 1.4.

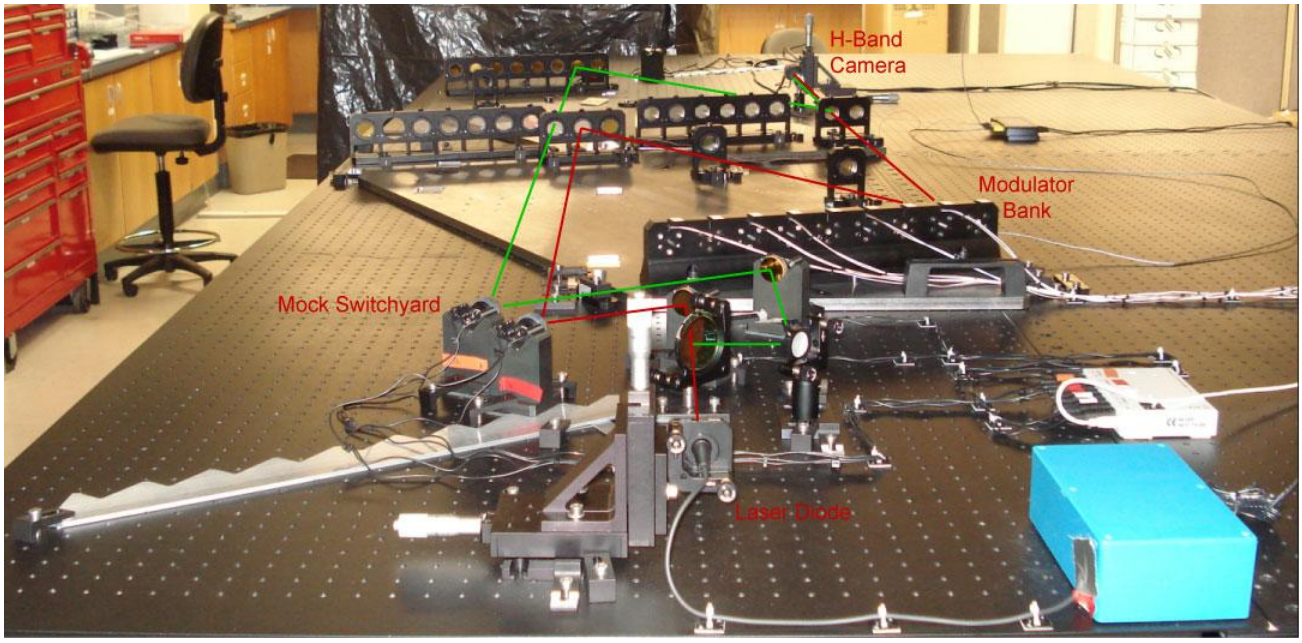

Figure 7. Initial set-up using an IR laser diode. Light from the diode is split into two paths before being injected into the mock switchyard. The mock switchyard mirrors can be positioned to any two combiner inputs, and likewise the H-Band camera can be moved to any output. The fiber-based white light injection system will be installed later this summer.

3. INITIAL RESULTS

Initial test results reported on in this paper are concerned with the following:

1. Verification of internal alignment methodology
2. Initial mechanical stability tests
3. Laser fringe visibilities

The remainder of the tests outlined in Section 2.1 will be conducted following the installation of the fiber-based white light injection system.

3.1 Internal Alignment Methodology

Inspection of the schematic illustrating the combiner architecture (Figure 2 right), reveals that the 39 individual optics are positioned within nine common optical planes. This architecture lends itself to a modular design philosophy whereby optics be placed within common planes, and then those planes be positioned and oriented with respect to one another. Figure 8 is an overview of the combiner hardware. Optics are placed in cells which are slid into modules (anodized mounts) with other optics that share a common plane. These modules are then located in position and orientation on two large steel plates that contact one another along two perpendicular edges. The plates are aligned in position and orientation to a reference laser using push-pull screws, and then bolted to the optical table.

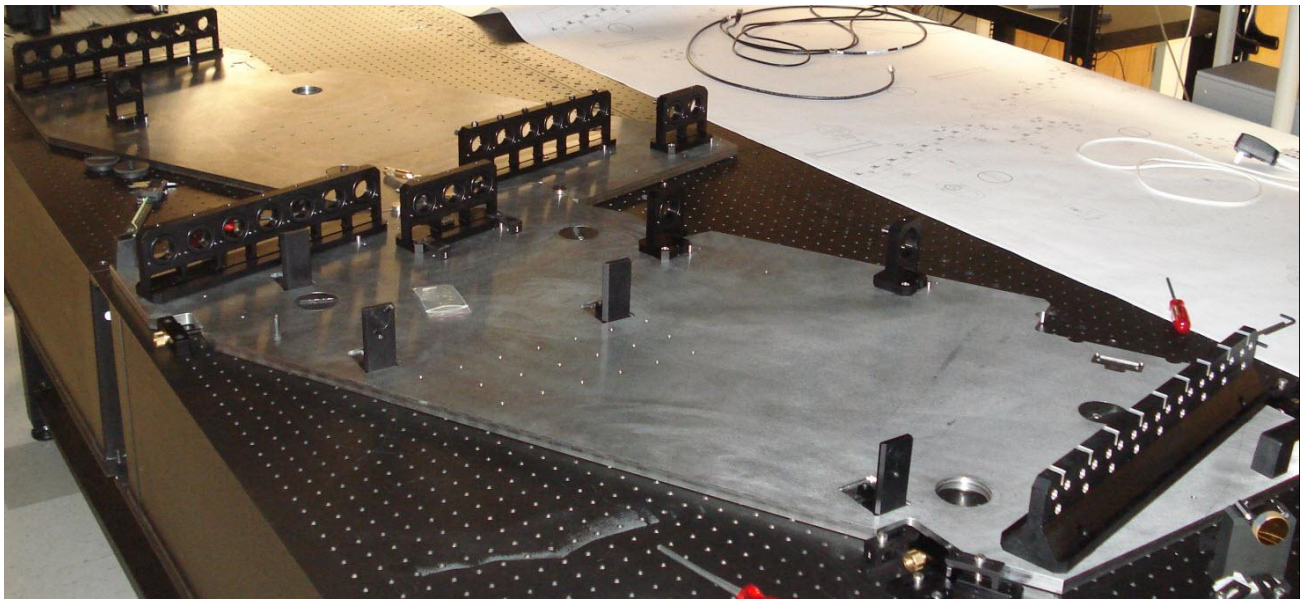

Figure 8. Modularity of the beam combiner. Optics are placed in cells which are slid into modules (anodized mounts) with other optics that share a common plane. These modules are then located in position and orientation on two large steel plates that contact one another along two, perpendicular edges. The plates are aligned in position and orientation to a reference laser using push-pull screws, and then bolted to the optical table.

This design approach was taken to minimize the number of internal adjustments and increase mechanical stability. In practice this works because each telescope input, and every combiner output has pair of mirrors to correct their trajectories:

1. The switchyard mirrors are used to remove tilt and shear errors between combiner inputs in the combination plane, regardless of their respective paths through the combiner.
2. The periscope optics are used to ensure the combiner outputs pass through the spatial filters in the spectrograph.

This does however require tight fabrication tolerances on the nine optic modules that define the common planes illustrated in Figure 2. Specifically, the modules must provide the following:

- Optic surfaces within a given module must be coplanar
- Plane defining optic surfaces must be perpendicular to the plane defining the base of the module
- Optic modules must be parallel to one another

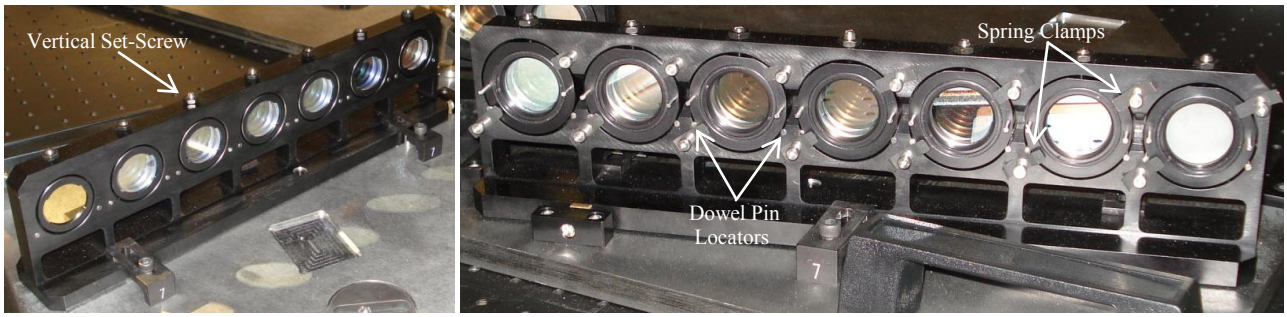

Figure 9. *Left:* Front surface of an optics module. *Right:* Back surface of the module. Locator dowel pins center the optic within the module, spring clamps press it into a common plane, and a vertical set-screw locks it in to place. Note that there are no individual optic adjustments.

Figure 9 shows two pictures of the front and back surfaces of one of the populated optics modules. The optical cells are centered within the module by two locator dowel pins; pressed into the same plane as the other optics with spring clamps; and locked into place by a vertical set-screw. Figure 10 shows the method by which the modules are clamped into place on the steel templates and then oriented with respect to the other modules. The location of each module on the template is indentified by a bullet-nosed pin. A receptacle at one end of the module is then press fit into place on the template, providing a pivot point about which the entire module can be adjusted in orientation.

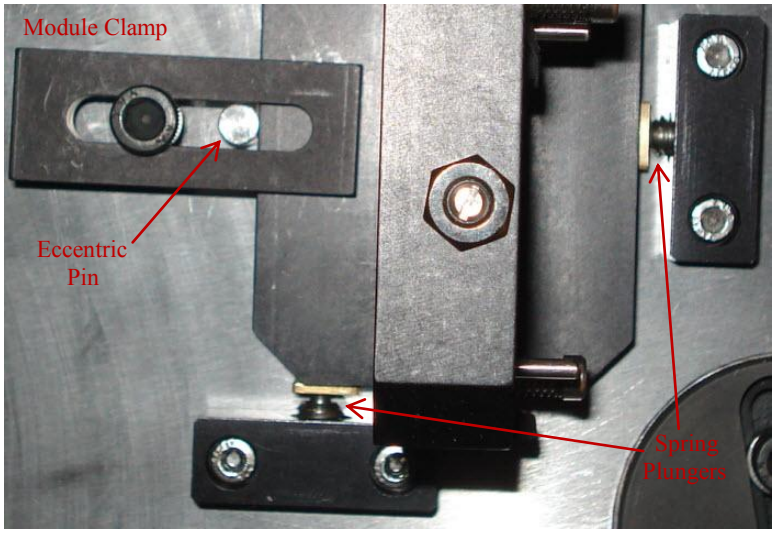

Figure 10. Each module is located on the steel alignment template by bullet-nosed pin. A second, eccentric pin has been press fit into the template at the opposite end of the module, allowing it to be adjusted in angle. Spring plungers constrain all modules to expand and contract (due to temperature changes) in the same direction.

A second, eccentric pin, is located at the opposite end of the module from the pivot point. The eccentricity of the pin allows the orientation of the module to be adjusted by rotating it. Every module in the combiner has this degree of freedom, and it is used to make all the modules parallel to each other. Spring plungers contact two perpendicular edges of the module, constraining all modules on the template to expand and contract (due to thermal changes) in the same direction. Finally, three L-shaped clamps lock the modules into place.

3.2 Stability Tests

For the stability tests, temperature probes were placed at five different locations on or around the combiner. Two probes were placed at either end of the combiner templates, and one was placed at the center where the two templates come in contact with one another. A fourth probe was suspended in air directly above the center of the combiner templates, and the fifth was located on the opposite side of the optical table, removed from the other probes. Figure 11 plots the temperature probe readings as a function of time for a total of 16 hours. In the figure, the three curves that track eachother are readings from the probes attached to the templates. The top curve is the probe that is on the opposite side of the table, and the curve that wanders between the template and removed readings are those from the probe suspended in air. In all cases, the temperature changes are on the order of 0.5°C. For reference, the temperature variation of the beam combining laboratory in the interferometer building has been measured to be less than 0.1°C over a similar period of time.

Concurrent to tracking the temperature, images of focused spots at a combiner output were taken every ten minutes. One of these images is shown inset at upper right in Figure 11. In this case, a lens with a focal length of 150mm was placed at the N1/N2 output (recall Figure 2) before the detector. The two input beams were intentionally misaligned in tilt so that the spots were adequately separated on the array. After the 16 hour period, the centroids of the spots were calculated, and their x/y pixel positions were plotted as a function of time. Figures 12 and 13 plot the motion of the spot centroids in the x/y directions. X1/Y1 is the centroiding of the spot at lower left in Figure 11, and X2/Y2 is the spot in the upper right. The time interval is the same as that for the temperature probe data. In both cases, the spots were calculated to have wandered by less than a pixel (~0.07mrad) in both x/y directions for a temperature change ~0.5°C. Longer term stability measurements (1 week) have begun, but not concluded in time for publication in this paper.

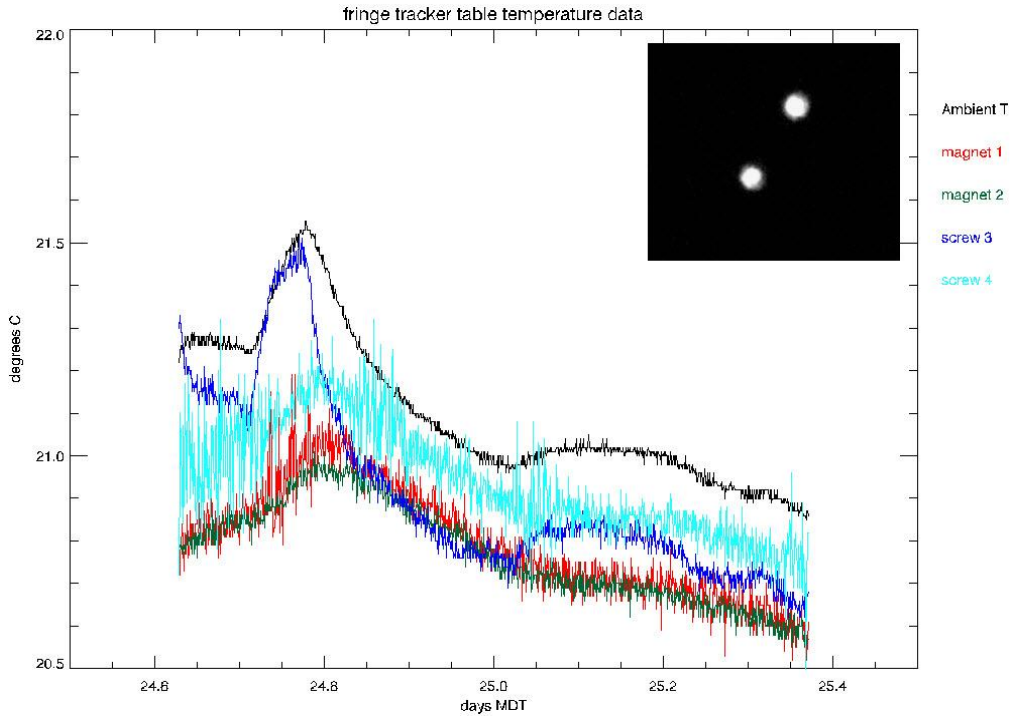

Figure 11. Temperature readings from the five probes placed on or around the combiner. All probes read temperature changes over the 16 hour period on the order of 0.5°C. This represents a worse case scenario since the temperature variation in the interferometer beam combination laboratory over a similar period of time has been measured to be much less than this (<0.1°C).

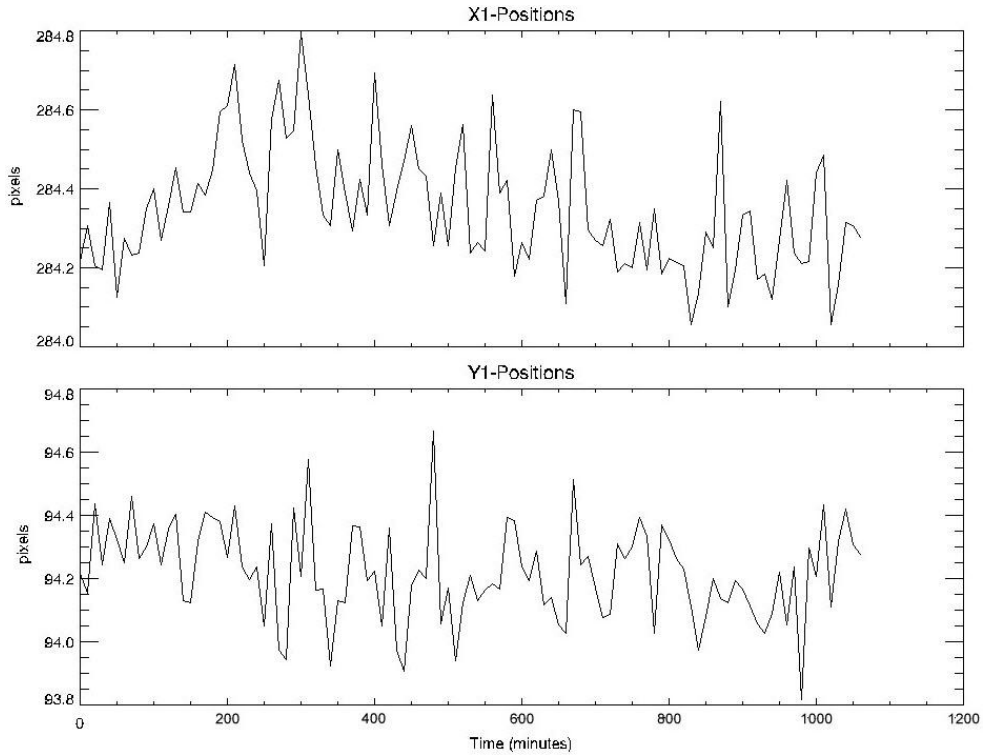

Figure 12. Centroid wander of spot 1 (lower left in Figure 11) was found to be less than a pixel (0.07mrad) for a temperature change, $\Delta T \sim 0.5°C$.

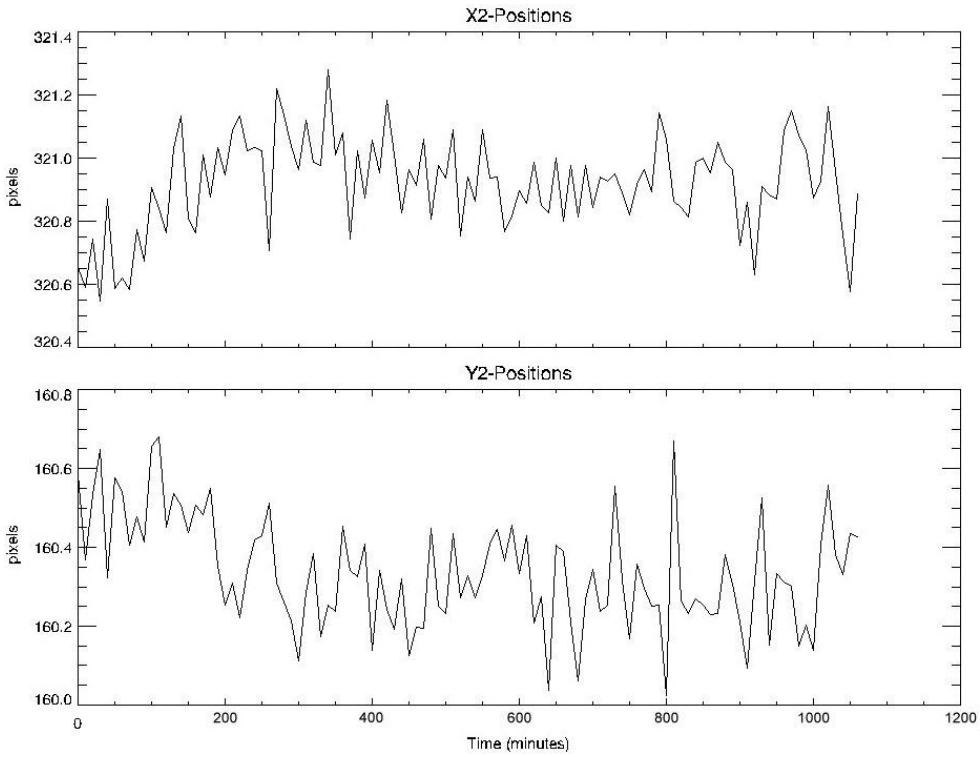

Figure 13. Centroid wander of spot 2 (upper right in Figure 11) was found to be less than a pixel (0.07mrad) for a temperature change, $\Delta T \sim 0.5°C$.

3.3 First Fringe Measurements

Figures 14 and 15 are the initial fringe measurements with the 1550nm laser diode on the six non-redundant combination paths through the combiner. In all cases, the calculated visibilities were within 1% of the ideal for this combiner architecture. For a detailed discussion about the six non-redundant combination paths through the combiner and their coating interactions see Nyland et al. in the references section of this paper.

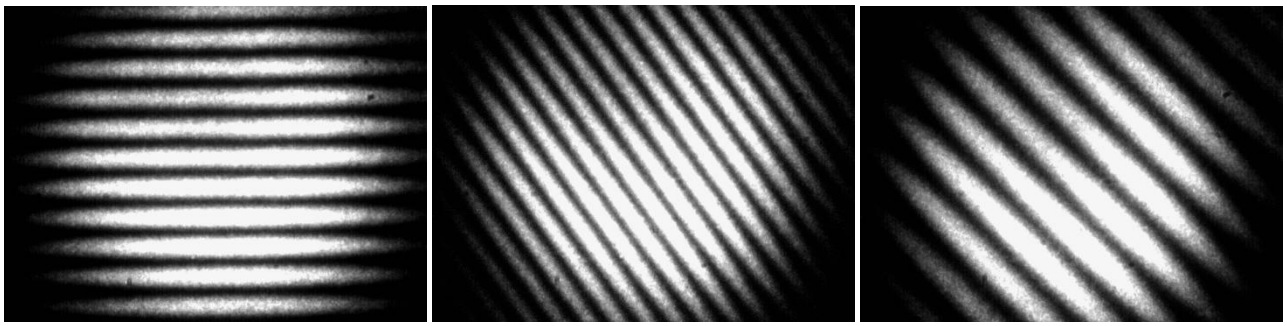

Figure 14. *Left:* S3 – S2 combination. *Middle:* S1 – W0 combination. *Right:* W1 – W0 combination.

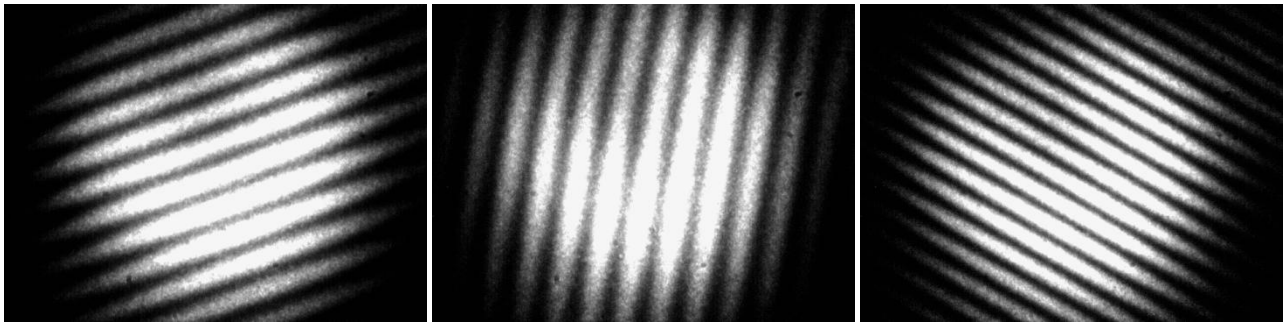

Figure 15. *Left:* W2 – W3 combination. *Middle:* W0 – N1 combination. *Right:* N1 – N2 combination.

ACKNOWLEDGMENTS

MRO is funded by Agreement No. N00173 – 01 – 2 – C902 with the Naval Research Laboratory (NRL). The MRO Interferometer is being built and managed by the New Mexico Institute of Mining and Technology (NMT) at Socorror, NM, USA, in collaboration with the University of Cambridge, UK.

REFERENCES

[1] Jurgenson, C., Santoro, F., Baron, F., McCord, K., Block, E., Buscher, D., Haniff, C., Young, J., Coleman, T., Creech-Eakman, M., "Fringe Tracking at the MROI," Proc. SPIE 7013, 70131C-1 (2008).
[2] Nyland, K., Jurgenson, C., Buscher, D., Haniff, C., Young, J., Lewis, J., Schmell, R., "Custom Beamsplitter and AR Coatings for Interferometry," this proceedings, 7734-141.
[3] Fisher, M., Boysen, R., Buscher, D., Haniff, C., Seneta, E., Sun, X., Wilson, D., Young, J., "Design of the MROI delay line optical path compensator," this proceedings, 7734-156.
[4] McCracken, T., Jurgenson, C., Seamons, J., McCord, K., Buscher, D., Haniff, C., Young, J., Baird, D., "Fringe Modulation for an MROI Beam Combiner," this proceedings, 7734-142.
[5] Shtromberg, A., Jurgenson, C., Bloemhard, H., Buscher, D., Farris, A., Haniff, C., McCord, K., Olivares, A., Torres, N., Santoro, F., "Magdalena Ridge Observatory Interferometer Automated Alignment System," this proceedings, 7734-39.